THE UNIVERSITY OF MICHIGAN

College of Engineering

Department of Mechanical Engineering

Cavitation and Multiphase Flow Laboratory

Report No. UMICH 01357-28-T

INVESTIGATIONS CONCERNING THE MODELING OF

FLOW CAVITATION*

Dr. Andreas P. Keller

Research Laboratory for Hydraulic Engineering,
The Technical University of Munich, Germany

Visiting Research Associate, Mechanical Engineering
Department, The University of Michigan.

*This is a summary of the doctoral thesis, "Experimentelle und
theoretische Untersuchungen zum Problem der modellmässigen
Behandlung von Strömungskavitation", carried through at the
Technical University of Munich, Germany

March, 1973

I. SUMMARY

Cavitation tests of submerged rotationally symmetric bodies of different shapes and diameters, carried out in connection with an optical measurement of cavitation nucleus spectra, show that cavitation inception is much influenced by the nuclei entrapped in the water. The investigations with four different qualities of test water let us conclude that diffusion plays no role in the nucleus motion, but that dynamic forces are responsible for the occurrence of scale effects.

The experimental results, as well as the theoretical investigations, support Harvey's pore model for cavitation nuclei in calm water.

Although the optical scattered-light procedure for determining nucleus size cannot distinguish between gas bubbles and solids, the results show that the measured nucleus spectra are in any case very informative.

II. INTRODUCTION

It is generally acknowledged that the "cavitation nuclei" entrapped in fluids are responsible for the occurrence of cavitation, and that knowledge of the size and population spectra of the nuclei is important for cavitation model tests. Hence, a measuring procedure for recording the nuclei spectra was developed based on their optical properties.

In connection with these optical measurements of the cavitation nucleus spectra, intensive investigations of cavitation inception on submerged bodies were carried out. The nuclei measurements and the cavitation tests will be

reported. It will be shown to what extent cavitation inception is influenced by the nuclei entrained in the fluid, and with the help of these results the utility of the optical measuring method for the recording of nuclei is discussed, as well as the validity of the nucleus pore model.

III. EXPERIMENTAL EQUIPMENT

For the cavitation tests, six different shapes of rotationally symmetric model bodies of three different diameters are chosen. From the different pressure distributions over the body contour and from the thus conditioned pressure gradients and boundary layer development, different forms of cavitation result. The influence of the total gas content and of the nucleus spectrum on inception shall be found (Fig. 1).

The model bodies represent a selection of shapes which cover the range from very well streamlined (2-caliber ogival) to extremely unstreamlined (blunt). The specific choice of the forms was decided by practical considerations.

Each body shape was tested in three different sizes with the diameters d = 60 mm, 45 mm and 30 mm. The upper limit of the model body size was determined by the dimension of the test section, the lower limit by the properties of the cavitation tunnel.

The bodies were manufactured from brass and were polished extra bright, so that the surface roughness was about R_s = 0.1 μm, where R_s signifies the maximum roughness of the profile. For the determination of the pressure distribution over the body contour, the two larger specimens

of each body family were supplied with six pressure taps. Thus with

the help of DMS-transducers the difference between the pressure p

along the contour wall, and the upstream pressure p_∞ in the flow at

different upstream velocities v_∞ could be measured. With the relation

$$K = \frac{p_\infty - p}{0.5 \varrho\ v_\infty^2}$$

the dimensionless pressure distributions could be determined. $K_{max.}$

occurs at the point of minimum pressure p_{min}. To find out the influence

of the nucleus content of the test water upon cavitation inception, the model

bodies were examined for the beginning of cavitation in tap water of

different qualities. By filtering and/or degassing of the water its content

of solids and dissolved gas was varied, and thus four different qualities

of water produced.

The number and size of the nuclei down to the range of $3 \mu m$ radius

were measured by an optical scattered-light method which is described in

detail in refs. 3 and 4.

For the objective measurement of cavitation inception on the sub-

merged bodies, likewise an optical method was utilized. This technique,

described also in ref. 3, facilitates the recording of single cavitation events

at a defined place.

The total gas content of the tunnel water was determined just after

each test run. Using a conventional form of a Van Slyke apparatus,

the water samples were drawn from the tunnel and tested.

The water velocity in the test section was determined from the pressure difference across the nozzle of the tunnel and recorded with help of a differential pressure transducer.

IV. RESULTS OF THE MEASUREMENTS

In order to ascertain the pressure distributions along the body profiles at different water velocities, the pressure difference between body surface and undisturbed flow was measured at six points of both the larger bodies of each model family. The pressure level of the tunnel was thereby set to the highest possible value (2 bar), to suppress cavitation as long as possible. In Fig. 2-7 the measured dimensionless pressure distributions of the six families are shown. The pressure values K are plotted against the contour, which is evaluated from the distance along the bodies. The position of the pressure taps can be seen from the sketches of the different bodies.

The body with the smallest K-value (K_{max} = 0.32), and therefore the most streamlined, proved to be the 2-caliber ogive. (Fig. 2). The K-values of the two bodies for which contour pressures were measured differ only very little at different velocities or Reynolds numbers. Thus only the two measured extreme pressure profiles are plotted.

Almost as streamlined is the halfbody (Fig. 3). For comparison with the measurements, there is plotted the computed pressure profile ($K_{max\ comp}$ = 0.33; $K_{max\ meas}$ = 0.4), and the one which deviates most from this. As the K-values of the spherical shape indicate (Fig. 4), this form is much less streamlined than the both preceding ones, but the measured

pressure distribution at different Reynolds numbers still lies relatively close.

It was found that the body with the next bigger K-value (K_{max} = 0.7 to 0.9) was that with the worst hydrodynamical shape, namely the blunt body. Here the K-values do not reach such a large maximum, but this maximum value is held over a relatively longer distance on the contour. The 1/8-caliber ogive bodies reach a much higher K_{max} (K_{max} = 0.8 to 2.2), than do the conical and especially the blunt bodies. Also there is much higher dependence of the pressure distribution on Re-number than for the conical and blunt bodies. These observations can be explained, however, by boundary layer considerations (e.g. ref. 10).

As above mentioned, the cavitation tests were carried out with four different qualities of test water. For the first test series, the tunnel was filled with untreated tap water. The degree of gas saturation (gas content compared to saturation at STP) for that water is between ξ = 1.3 and ξ = 1.15, after having been settled for some time (temperature 20°C; atmospheric pressure $\xi = \dfrac{C_o}{C_s}$, C_o = measured gas, C_s = quantity of gas at saturation). The water was therefore slightly oversaturated for STP conditions; for conditions at cavitation inception, it was naturally much oversaturated. Figure 8 shows a nucleus histogram for that water sample. The number N_{tl} (total recorded nuclei with radius larger than R = 3 μm) was 379. Nine nuclei were registered with R larger than 23 μm. During the measuring time of 120 sec. the volume of water tested was 1.3 cm.^{3} Thus the nucleus concentration per cm^3 was to N = 291.5 and $N_{R > 23\,\mu m}$ = 6.9.

In Fig. 3 the nucleus spectrum of the same water under the same

external conditions can be seen, after it had been degassed to a portion of

saturation at STP of $\varepsilon = 0.35$. The nucleus content for the water of the secor

test series amounts to $N_{tl} = 235$, $N = 180.8$ and $N_{R>23\,\mu m} = 0.75$ nuclei per cm

The number of measured nuclei is therefore about 35% lower

than for the gas saturated water, and there exist nearly no

nuclei with radii larger than $R = 23\,\mu m$ in this case. Obviously by outward

diffusion of gas in this under-saturated water, the gas nuclei are reduced

so far that altogether 111 n uclei per cm^3 were removed from the measured ran

and no nuclei existed above the limit of $R = 23\,\mu m$.

Examples for the nuclei spectra as they were recorded for the water

of the third and fourth test series, namely filtered water, can be seen in

Fig.10. There only 19 nuclei below $R = 23\,\mu m$ were measured, corresponding

to $N = 14.6$ nuclei/cm^3. In spite of filtering with a filter of a nominal pore

size of $0.5\,\mu m$, the water still contained particles with $R > 0.25\,\mu m$.

This is probably because of not being able to completely clean the tunnel

of contaminant particles.

The nuclei spectra shown in Fig. 8 through 10 are randomly picked

examples of several measurements made respectively of the same water after

the treatment last described. The measured nuclei are subjected to

stochastical laws, so that the nucleus concentration from a single measure-

ment deviates more or less from the mean, according to the volume examined

by the water probe (dependent on the measuring time) and on the nucleus

concentration. Thus the reproducibility of the nuclei spectra of unfi ltered

water was very good, for the difference from the mean value was a maximum

of 5%, so that the measuring time of 120 sec for that water is sufficient.

On the other hand, the water sample of 1.3 cm^3 tested within the 120 sec. was too small for the filtered water. Thus the scatter of the measured nucleus concentration of the same water was relatively high (up to 50% of the mean value). Therefore, a difference between gas saturated filtered water and degassed filtered water could scarcely be established. For this reason, only one sample for the nuclei spectra of filtered water is shown.

With the help of the optical method, cavitation inception for the 18 model bodies was investigated with the four different qualities of the water. The preparation of one experiment and the test run itself was carried out in the following way. After having installed a model body, the tunnel was filled and the total gas content was measured. In order to eliminate all bubbles from the tunnel which were not entrapped in the water, the water was circulated for several passes. Then at a certain tunnel pressure, the water was settled for about one hour, and the nuclei stabilized. Next, at very low circulation speed the nuclei spectra were measured, and subsequently the water was accelerated and cavitation inception recorded. Cavitation inception was determined before the water had finished one complete pass, after which "disturbed water" with a changed nucleus spectrum would come into the test section.

In Fig. 11 to 16 the cavitation number σ_v referred to vapor pressure $\sigma_v = \dfrac{P_\infty - P_v}{0.5 \rho V_\infty}$ is plotted against Reynolds number (Re = $\dfrac{V_\infty \cdot d}{\nu}$). Thus the influence of different body sizes and nuclei spectra becomes very clear.

The range of Reynolds number was determined only by the body sizes. The upstream static pressure in the tunnel was the same for all tests, namely 1 bar. Usually in cavitation tests one covers the Reynolds range by altering the static pressure. But in doing so, one changes the nuclei spectra too, but in an uncontrolled way, so that one has no comparable results. For our investigations, however, the nuclei spectra at cavitation inception of one water quality was for each test run the same.

Besides the σ_v -values, the measured K_{max} of each body at the different Re-numbers were plotted in Figs. 11 to 16. Thus one can see the dependence of the parameter K on Re-number. For streamlined bodies, it is as expected very little. On the other hand, for unstreamlined shapes it is considerable.

However, while considerating these results one must remember that the pressure distribution is measured at the contour of the bodies. Thus especially for the unstreamlined bodies, one measures K-values which are too small, since at the center of vortices in the turbulent boundary layer in the zone of detachment, certainly lower pressures occur than at the contour of the bodies. This is also the reason that (at least in water with many cavities), the σ_v -values for streamlined bodies are always smaller than the K_{max} -values, measured at the contour. For unstreamlined bodies, however, the σ_v -values are larger.

V. DISCUSSION OF THE RESULTS

A. Nuclei Spectra and Cavitation Inception

The nuclei spectra shown in Fig. 8-10 indicate that the nucleus content of water can be varied by filtering and/or degassing. While an alteration of the total gas content affected the measured nucleus spectrum only moderately, many nuclei were withdrawn from the water by filtering.

As already mentioned, in spite of filtering with a filter of 0.5 μm nominal pore size, nuclei still exist in the water with diameters larger than 0.5 μm since even after several rinsings with filtered water, the tunnel still contains larger particles in various stagnent regions, crevices, etc.

Figures 11-16 (Cavitation number vs. Re-number) show the following. For the streamlined bodies (2-caliber ogive and halfbody) cavitation occurs first in unfiltered, gas saturated water; then in unfiltered, degassed water; and finally in filtered water. Nearly no difference can be found between gas saturated and degassed water.

However, for the spherical-nosed bodies, and more distinctly for the completely unstreamlined shapes, another sequence is observed. Naturally here too the unfiltered, gas saturated water cavitates first, but the next most susceptible to cavitation is the unfiltered degassed water, replacing thus the filtered, gas saturated water. That most resistent to cavitation proved to be in all tests the filtered, degassed water. This difference in behavior between streamlined and unstreamlined bodies is explained in the following.

Because of considerations of stability for various nucleus models, one can suppose that only in conical pores at the boundaries of the flow, and/or for suspended particles under certain assumptions, can cavities stabilize as cavitation nuclei under all conditions. In making static and dynamic stability studies for these pore nuclei (see appendix) one finds that, above all, the aperture radius of the pore R_p plays a role in determining the amount of the critical pressure. R_p is the minimal radius of curvature which the phase boundary can achieve on the development of the cavitation bubble. It determines, therefore, the degree of the pressure decrease below vapor pressure to reach the critical point for bubble growth, beyond which no stable equilibrium can exist. The total gas content has an influence upon the behavior of the nucleus only when the pressure decreases to near the vapor pressure.

These ideas are confirmed by the measuring results at the bodies with smooth pressure gradients (2-caliber ogive and halfbody shap There is practically no difference in the cavitation inception behavior for gas saturated and well degassed, filtered water.

For the bodies with steeper pressure gradients however, beginning with the spherical nosed form, the cavitation inception sigma is quite different depending on the total gas content. Unfiltered water shows (even for the stream-lined bodies) a dependency upon total gas content.

These results lead, therefore, to the conclusion that friction, accelerati and viscous forces can have a substantial influence upon the growth of a bubble.

This is easy to comprehend, if one considers that by subjecting a pore nucleus to a short duration underpressure, in the case of gas saturated water, the phase boundary rapidly attains the border of the pore, and, therefore, the critical condition for growth can be reached very quickly. However, in the case of degassed water, the phase boundary must move from the bottom of the pore. A substantial time may be required, depending on pressure gradient and depth of the pore.

The assumptions that,(above all),inertia and friction, but no diffusion processes, affect the course of phase boundary motion for a pore nucleus under dynamical stress, is supported too, by the results of Knapp (5), Holl (2), Reed (9) and others. They found that water submitted to high pressures (up to 1000 bar) could resist for some time high tensile stresses, compared to untreated water; the susceptibility to cavitation being thus diminished considerably. By such over-pressure the phase boundary in the pores (which are included as suspended particles or on flow boundaries) is pushed back, achieving the same effect as degassing.

Although the Reynolds range which is covered by the three model body sizes is relatively small (Re-number between 10^5 and 10^6) one can recognize a dependency of the σ_v-value for the same water qualities, which exceeds the dependency of the K_{max}-values measured at the body contour. As computations confirm (appendix), this is due to inertia and friction effects affecting the nucleus movement. However, one must remember that the computations are based on the pressures measured at the body contours.

At this point it is perhaps convenient to come back once more to the problem of evaluating the K_{max}-value from the pressures measured on the contour of the submerged bodies. At cavitation inception the measured pressures were below the vapor pressure only for the streamlined bodies; 2-caliber ogive, halfbody, and the spherically-shaped bodies. For the other three body shapes, the minimum pressure measured at cavitation inception is considerably above the vapor pressure, (see Table I)

Body-Form	2-Caliber-Ogive	Half-Body	1/2 Caliber Ogive	Con-ical	1/8-Caliber Ogive	Blunt
P_{min} (bar) (d=60 mm)	-0.016	-0.010	-0.15	0.15	0.04	0.37

Table I - Minimum Measured Pressures on the Body Contour at Cavitation Inception at the Bodies with d = 60 mm in Untreated Water.

This result forces one to the conclusion that in the turbulent boundary layer, i. e., in the shear layer between the zone of detachment and the laminar flow approaching the body* , lower pressures may occur than at the body surface. As high speed photographs show, for unstreamlined shapes, cavity formation does not begin at the contour, but in the center of the turbulent vortices at a relatively large distance from the flow boundary (4).

The K_{max}-value evaluated from the pressures measured on the body contour is, therefore, for such flow conditions too small. It must be developed from the minimal pressure at the point of actual cavitation (see Ref. 7).

---

*made laminar by honeycomb.

This is the explanation for the cavitation numbers σ_v for cavitation inception on streamlined bodies being always less, and those for unstreamlined bodies being always larger than, the K_{max}-value, at least for untreated water.

The fact that cavity formation occurs even though the minimum pressure measured on the submerged contour is not below the vapor pressure, i.e., $\sigma_v > K_{max}$, often is explained as degassing (gaseous cavitation), e.g. ref. 2 and 6. This may be true if the flowing liquid contains bubbles for which the critical radius has already been exceeded. However, it is not clear why the nuclei in water of the same quality and for the same exterior conditions in the case of a streamlined body, became unstable at pressures below the vapor pressure, while on the other hand, unstreamlined bodies cavitate above the vapor pressure, although the stay-time for the nuclei in the zones of minimum pressure are nearly the same.

B. Optical Measuring Method for Nuclei

By comparing the measured nuclei spectra with cavitation inception sigmas for both streamlined shapes with smooth pressure gradient, it was roughly estimated how far the optical nucleus recording can give actual information about the nucleus size, although it can not distinguish between bubbles and solid particles. With the help of the measured minimum pressure at the body contour P_{min}, and of the static equilibrium conditions (see appendix) the corresponding critical radius of the hypothesized pore crevice $R_{P, crit}$ can be calculated. (See Table II).

| | 2-Caliber Ogive | | | | Half Body | | | |
| | Filtered Water | | Unfiltered Water | | Filtered Water | | Unfiltered Water | |
d (mm)	P_{min} (bar)	$R_{p,crit}$ (µm)	P_{min} (bar)	$R_{p,crit}$ (µm)	P_{min} (bar)	$R_{p,crit}$ (µm)	P_{min} (bar)	$R_{p,crit}$ (µm)
60	-0.48	2.8	-0.016	24	-0.27	4.7	-0.010	26
45	-0.50	2.7	-0.058	14	-0.39	3.4	-0.054	15
30	-0.50	2.7	-0.117	9	-0.41	3.2	-0.084	11

Table II - Measured Minimum Pressures P_{min} on the Body Contour of 2-Caliber Ogive and Half Body Models at Cavitation Inception in Filtered and Unfiltered, Gas Saturated Water and Derived Critical Pore Radii $P_{p,crit}$

If one compares now the calculated pore radii for cavitation inception for the large streamlined bodies (as explained above, these can be the only suitable ones for that purpose because then the static conditions are approximated the best) with the measured nuclei spectra, one comes to a surprising result. The biggest nuclei measured with the optical method and the theoretically evaluated crevice radii roughly correspond, this though _ nuclei in still water can exist only with suspended particles for which the gas filled cavity must be at least partly inside the pore.

This correspondence in size between crevice and gas nuclei can be explained only if one assumes that the scattered intensity of a porous, gas filled particle is about the same as for spherical bubbles with a radius equivalent to the radius of the crevice. Even though the gas nucleus is partly (in gas saturated water) or completely (in degased water) hidden in the pore, the scattered light from the solid delivers approximate information on the dimension

of the pore nuclei. Evidently big particles are carriers of big crevices and small suspended particles are carriers of small ones. This is obvious, since the particles suspended in water are surely not spheres, containing a tiny pore, but have irregular shapes, and thus form an arbitrary crevice of size depending on the total size of the particle.

In this context the results of the work of Brossmann (1) will be mentioned. There, eight different sorts of particles were tested for their optical scattering properties, and the dependence of the scattered intensity from the position of the particle was investigated. It was found that particles with rough surface, or inhomogenous particles i.e. particles which admit diffuse light spreading

inside because of their inhomogenous composition, show only a small alteration of scattered light in changing their position against the incident light. This is true for transparent as well as for absorbing substances. Their scattering properties are therefore like those of spheres.

Therefore, one can say that, although this optical procedure for determining the nucleus size cannot distinguish between gas bubbles and solid particles, the nucleus spectrum so measured is still very informative. In gas saturated or slightly over—saturated calm water, i.e., with stabilized pore nuclei, for which the phase boundary is fixed at the boundary of the pore, the measured nucleus radius can be equated to the pore radius. In degassed pressurized water the measured nucleus spectrum gives information about the suspended particles in the water. The measured radii related to an equivalent spherical bubble correspond roughly with the radii of the hypothesized crevices in the suspended particles. Concerning gas filled cavities hidden completely within the pores, nothing can be said except on theoretical

grounds, taking into account the degree of gas saturation, external pressure, angle of wetting and angle of the crevice. However, because the critical pressure is determined predominantly by the radius of the crevice aperture in the nucleus-carrying particle, even approximate knowledge is a great help for judging the tensile strength of the water.

APPENDIX

In order to have a possibility of comparing the measured results with pore properties, the following investigations were carried through.

a) Static equilibrium of pore nuclei

Conical pores (crevices) in flow boundaries of suspended particles with opening angle $\psi < \lambda \; \vartheta - \pi$ (ϑ = wetting angle) can stabilize gas filled cavities as cavitation nuclei even in liquids unsaturated with gas, and liquids at high external pressures. The equilibrium condition for such pore nuclei is

$$P_a = P_i + \frac{2\sigma}{R_{Kr}} \tag{1}$$

The radius of curvature R_{Kr} of the phase boundary results from geometrical considerations because of the following relations:

$$\alpha = \pi - \left(\vartheta - \frac{\psi}{2} \right)$$

for

$$R_{Kr} = \frac{r}{\cos \left(\vartheta - \frac{\psi}{2} \right)} \tag{2}$$

r can vary between 0 and R_p (see Fig. 17.).

For wetting angles $\vartheta > \frac{\psi}{2} + \frac{\pi}{2}$ R is negative, i.e., the phase boundary is concave against the liquid. Since R_{Kr} is able to achieve any small value, the capillary pressure 'p' acting towards the center of the curvature in practice can compensate for any external pressure, whereas the phase boundary recedes to the bottom of the pore. On the other hand, it approaches the boundary of the pore for pressure reductions and reaches it a

$$P_a = P_i + \frac{2\sigma}{R_p} \left[\cos \left(\vartheta - \frac{\psi}{2} \right) \right] \tag{3}$$

At further pressure reduction, the negatively curved segment of the bubble

becomes flat and seals the pore aperture even at $p_a = p_i$. For $p_i > p_a$

the curved segment of the bubble wall arches outside, until an equilibrium

is reached in the range of

$$P_i - \frac{2\sigma}{R_{Kr}} = P_a > P_i - \frac{2\sigma}{R_p}$$

This equilibrium will be destroyed if the minimum radius $R_{Kr, min} = R_p$

is exceeded.

The inside pressure p_i of the cavity includes the vapor pressure of

the water p_v and the partial pressure of the contained gas, p_g, which can

be found from Henry's law

$$p_g = {}^c o / \alpha_B$$

c_o = Concentration of dissolved gas

α_B = Bunsen's absorption coefficient

The partial pressure p_g during the expansion of the bubble can be evaluated

from the general gas law for isothermal state condition (Boyle-Mariotte)

$$p_g = {}^c o / \alpha_B \cdot \frac{V_o}{V}$$

V_o is the volume of the nucleus at rest formed by the pore and the phase

boundary. V is the volume of the cavity in an expanded stage.

The pressure part caused by the surface tension p_σ of the water is to be

calculated for each possible position of the phase boundary. If the boundary

has not reached the pore boundary, the partial pressure p_σ is

$$P_\sigma = \frac{2\sigma}{R_{Kr}} = \frac{2\sigma}{r} \left[\cos(\vartheta - \tfrac{1}{2}) \right]$$

The phase boundary reaches the pore border, and then the wetting

angle plays no role, so that

$$P_a = \pm \frac{2\sigma}{R_{Kr}}$$

depending on the direction of the curvature. Equation (2) can now be

written as

$$P_a = \frac{C_o}{\alpha_B} \cdot \frac{V_o}{V} + P_v \pm \frac{2\sigma}{R_{Kr}} \tag{4}$$

In order to have a uniform quantity for all crevice shapes, the spherical

volume with radius R_e will be assumed equivalent to the volume of the cavity.

The radius of R_e of this spherical equivalent can be computed with the help

of equation (5) for the case that the boundary has not reached the border

$$R_e = r \sqrt[3]{\frac{1}{4}\left(ctg\frac{\varphi}{2} - \frac{(1-\sin\ (\vartheta-\frac{\varphi}{2}))^2(2+\sin\ (\vartheta-\frac{\varphi}{2}))}{|\cos\ (\vartheta-\frac{\varphi}{2})|^3}\right)} \tag{5}$$

Equation (6) applies for the case that the boundary is fixed at the pore border.

$$R_e = \sqrt[3]{\frac{1}{4}\left(R_p^3\ ctg\frac{\varphi}{2} \pm R_{Kr}^3\ (1-\sin\ (arc\ \cos\frac{R_p}{R_{Kr}}))^2 \cdot (2+\sin(arc\ \cos\frac{R_p}{R_{Kr}}))\right)} \tag{6}$$

Figure 18 shows , some examples computed with the equations above.

One can remark at once that for the conditions assumed above, the minimum

pore radius R_p controls the critical pressure. The gas content has an

influence only down to a pressure near the vapor pressure.

b) Nucleus movement with dynamical tensile stresses

To check theoretically whether the time factor does play a significant role in the growth of a pore nucleus as it passes a submerged body, the volume alteration of the nucleus under conditions of dynamical strain of the fluid, i. e. at temporally changing tensile stress must be investigated.

For the growth of the gas cavity in a pore nucleus in the first approximation, it can be assumed that the liquid in the crevice moves radially away from the bottom of the crevice. Therefore, the basic equation for the gas nucleus movement is the well known differential equation of second order, which has been evaluated from Euler's equation of motion and the equation of continuity (e.g. 6)

$$R \frac{d^2 R}{dt^2} + \frac{3}{2} \left(\frac{dR}{dt} \right)^2 = \frac{1}{\rho} \left(P_R - P_\infty \right) \tag{6}$$

$P_R - P_\infty$ is the difference between the pressure of the fluid at the bubble wall, and the pressure in the surrounding liquid. R is here the position of the water interface from the bottom of the pore. Integration of Eq. (6) is only possible with special assumptions of the pressure. If the pressure is given in a general form, this expression must be integrated numerically.

The viscosity of the fluid causes a damping of the motion of the phase boundary for the growth and collapse of the cavity. A term is added to eq. (6) to consider the viscous effect as derived from the Navier-Stokes equation (8).

$$\frac{4\mu}{\rho} \frac{1}{R} \frac{dR}{dt}$$

The pressure at the phase boundary is (see reflections section a)

$$P_R = \frac{C_o}{\alpha_B} \cdot \frac{V_o}{V} + P_V \pm \frac{2\sigma}{R_{k\nu}}$$

Here again it is necessary to distinguish whether the phase boundary arches outward (negative sign of $\frac{2\sigma}{R_{k\nu}}$) or inside (positive sign) and whether it is fixed at the border of the pore or not.

Finally the equation which was used for computing the motion of the phase boundary is

$$R \frac{d^2 R}{dt^2} + \frac{3}{2} \left(\frac{dR}{dt} \right)^2 + \frac{4\mu}{\rho} \cdot \frac{1}{R} \cdot \frac{dR}{dt} = \frac{1}{\rho} \left(\frac{C_o}{\alpha_B} \cdot \frac{V_o}{V} + P_V \pm \frac{2\sigma}{R_{k\nu}} - P_\infty \right) \quad (7)$$

Such influences as friction of the boundary layer at the inside of the pore, gaseous diffusion and thermal effects, are not taken into consideration.

To investigate the effects of inertia and friction forces as well as the gas content upon the growth of pore nuclei, some nucleus models have been exposed to pressure histories with different pressure gradients. For the computation of equation (7) the Runge-Kutta procedure was used.

The volume of the cavity was again converted to a spherically equivalent volume and the equivalent radius is plotted against the pressure. The change in the nucleus size(until reaching the stagnation point (K = -1) of the main flow regime) was calculated considering equilibrium properties to apply, because the pressure changes happen relatively slowly. The computation of the nucleus motion under dynamical stress in the pressure field at the body contour begins at K = -1. The pressure profile was taken as it was measured along the bodies. The critical equivalent radius, i.e., the beginning of cavitation was defined when the radius of curvature of the phase boundary arching outside, has reached the radius of the pore aperture R_p.

In Fig. 19 the computed course of the equivalent radius of a pore nucleus with radius of crevice R_p = 20 μm, the opening angle γ = 100°, and the wetting angle ϑ = 150° in a water of degree of saturation ξ = 1 and flow velocity v_{∞} = 14 m/s is plotted against the pressure p. The behavior of a nucleus in the pressure field of a half body, i.e. in a pressure field with smooth pressure gradient, shows the curves (a) for body diameter d = 12 cm, and (b) d = 1.5 cm. The influence of the inertia force here is not yet very big, so that it is not necessary to impose a pressure much below the static critic pressure $P_{crit\ stat}$ to reach the critical equivalent radius.

By crossing a pressure field with steep gradient, e.g. along the contour of submerged bodies of the form of the 1/8 caliber ogive, the inertia effect can be very considerable, as can be seen from the curves c-f. Thus an under pressure of about 0.4 bar must be applied to reach the critical equivalent radius.

In Fig. 20 the motion of a nucleus with R_p = 4 μm is shown. For the half body this nucleus does not cavitate at water velocities of 14 m/s. For the 1/8 caliber ogive body, this nucleus does cavitate. However, the pressure is only slightly below the static critical pressure. This result was expected, because smaller cavities have a higher frequency response than larger ones.

The influence of the gas content and of the opening and wetting angles were also computed. Their influence is very small.

A comparison between the measured nucleus spectra, measured cavitation inception sigma, and critical size of pore nuclei, (investigated by statical and dynamical equilibrium considerations) yields good agreement for the streamlined bodies. However, to make the dynamical pore model applicable to steeper pressure gradients, it must be improved, mainly by taking into account the flow properties inside of the crevice during the motion of the phase boundary. For an experimental reconsideration, however, the pressure properties of the turbulent flow around unstreamlined bodies must be known exactly.

BIBLIOGRAPHY

1. Brossmann, R. "Die Lichtstreuung an kleinen Teilchen als Grundlage einer Teilchengroessenbestimmung," Dissertation TH Karlsruhe, 1966.

2. Holl, J.W. "Nuclei and Cavitation," *Trans. ASME, J. Basic Engr.*, 92, D, Dec. 1970, p. 681-688.

3. Keller, A. "The Influence of the Cavitation Nuclei Spectrum on Cavitation Inception, Investigated with a Scattered Light Counting Method," *Trans. ASME J. Basic Engr.*, 94, D, 4, Dec. 1972, p. 917-925.

4. Keller, A. "Experimentelle und theoretische Untersuchungen zum Problem der Modellmaessigen Behandlung von Stroemungskavitation," Dissertation TU Muenchen, Feb. 1973.

5. Knapp, R.T. "Cavitation and Nuclei," Trans. ASME, 80, Aug. 1958, p. 1315.

6. Knapp, R.T., Daily, J.W., Hammitt, F.G. *Cavitation* (McGraw-Hill Book Company: New York, New York), 1970.

7. Koch, H.J. "Die Umstroemung der Quadratischen Schwelle im Rechteckgerin bei ueberkritischem Fliesszustand", Dissertation TU Berlin, Sept. 1972.

8. Poritsky, H. "The Collapse or Growth of a Spherical Bubble or Cavity in a Viscous Fluid," *Proc. First U.S. Nat. Cong. Appl. Mech.*, ASME, 1952.

9. Reed, R.L. "The Influence of Surface Characteristics and Pressure History on the Inception of Cavitation," M.S. Dissertation, Dept. of Aerospace Engineering, Pennsylvania State University, 1969.

10. Schlichting, H. *Grenzschicht-Theorie*, 3. Auflage, Verlag Braun Kralsruhe,
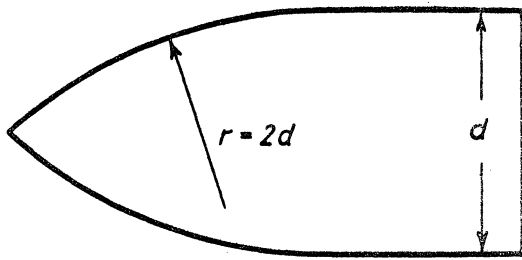
a) 2-caliber-Ogive
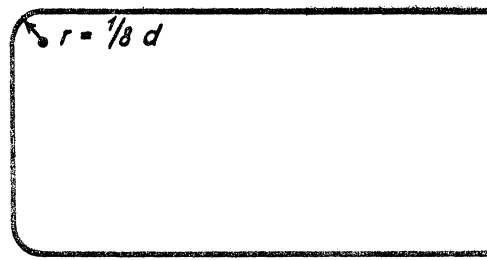
d) $^1/8$-caliber-Ogive
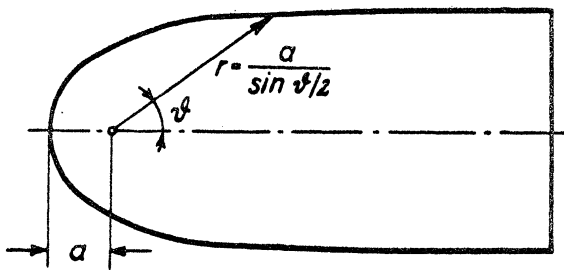
b) Half Body
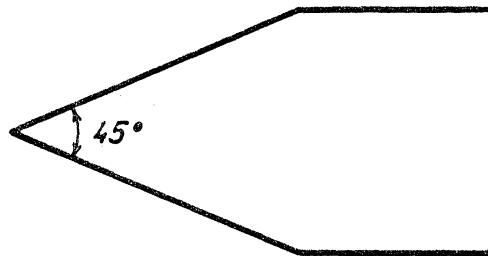
e) 45° conical
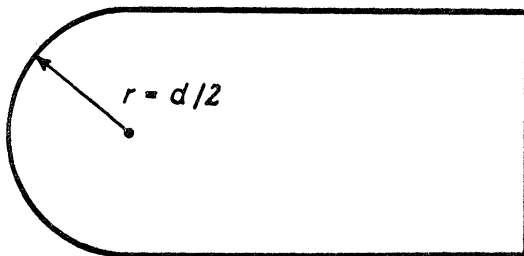
c) $^1/2$-caliber-Ogive
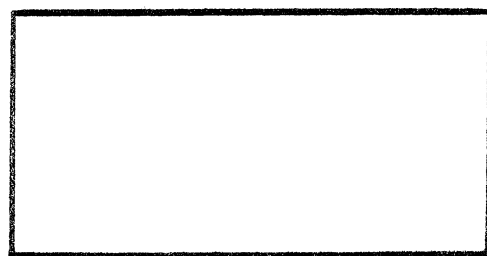
f) blunt

Fig. 1: The six body shapes investigated
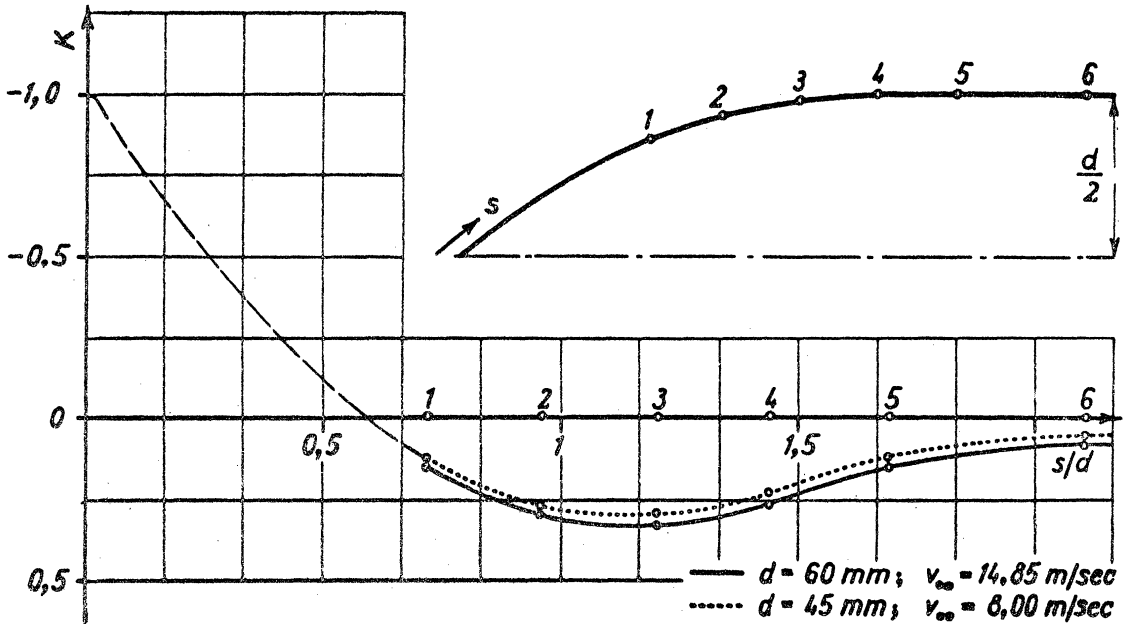
Fig. 2: Dimensionless pressure distribution at the 2-caliber ogive bodies
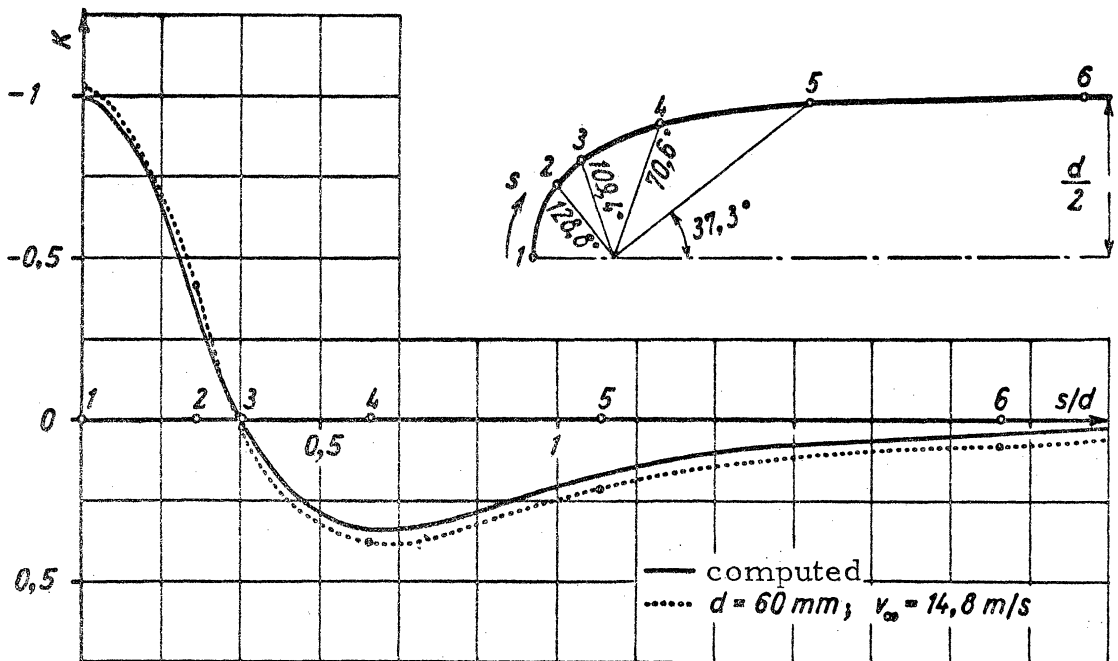
Fig. 3: Dimensionless pressure distribution at the half bodies
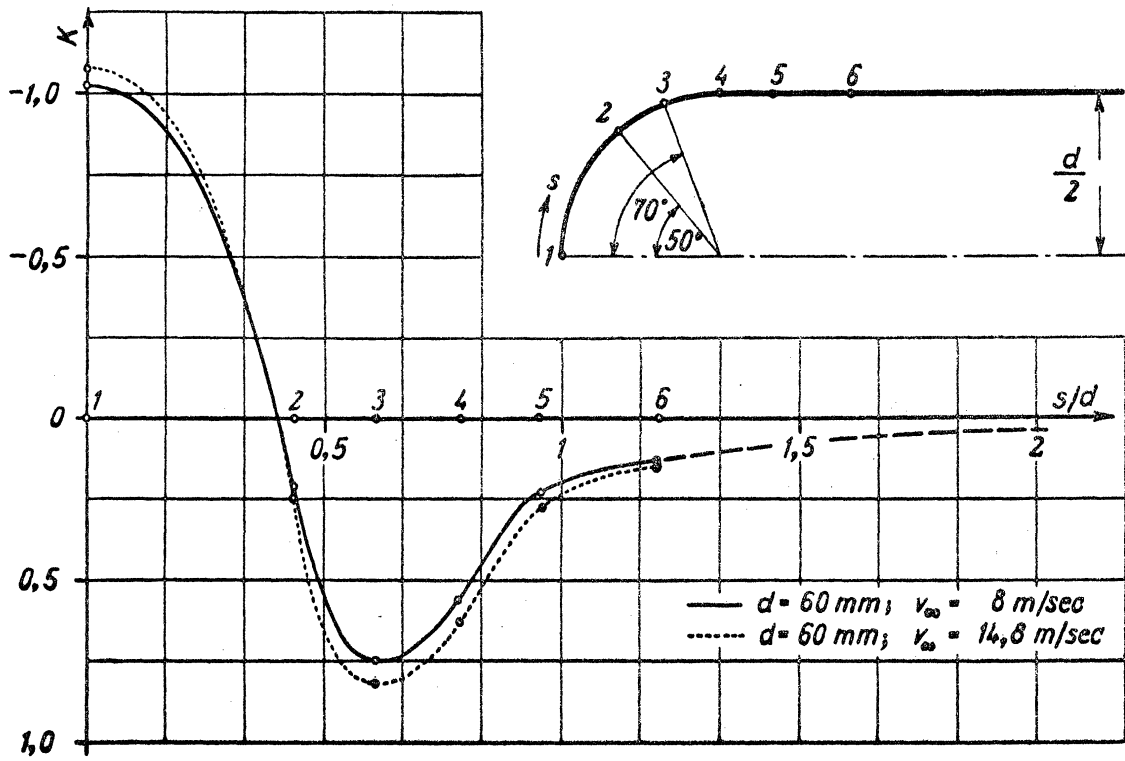
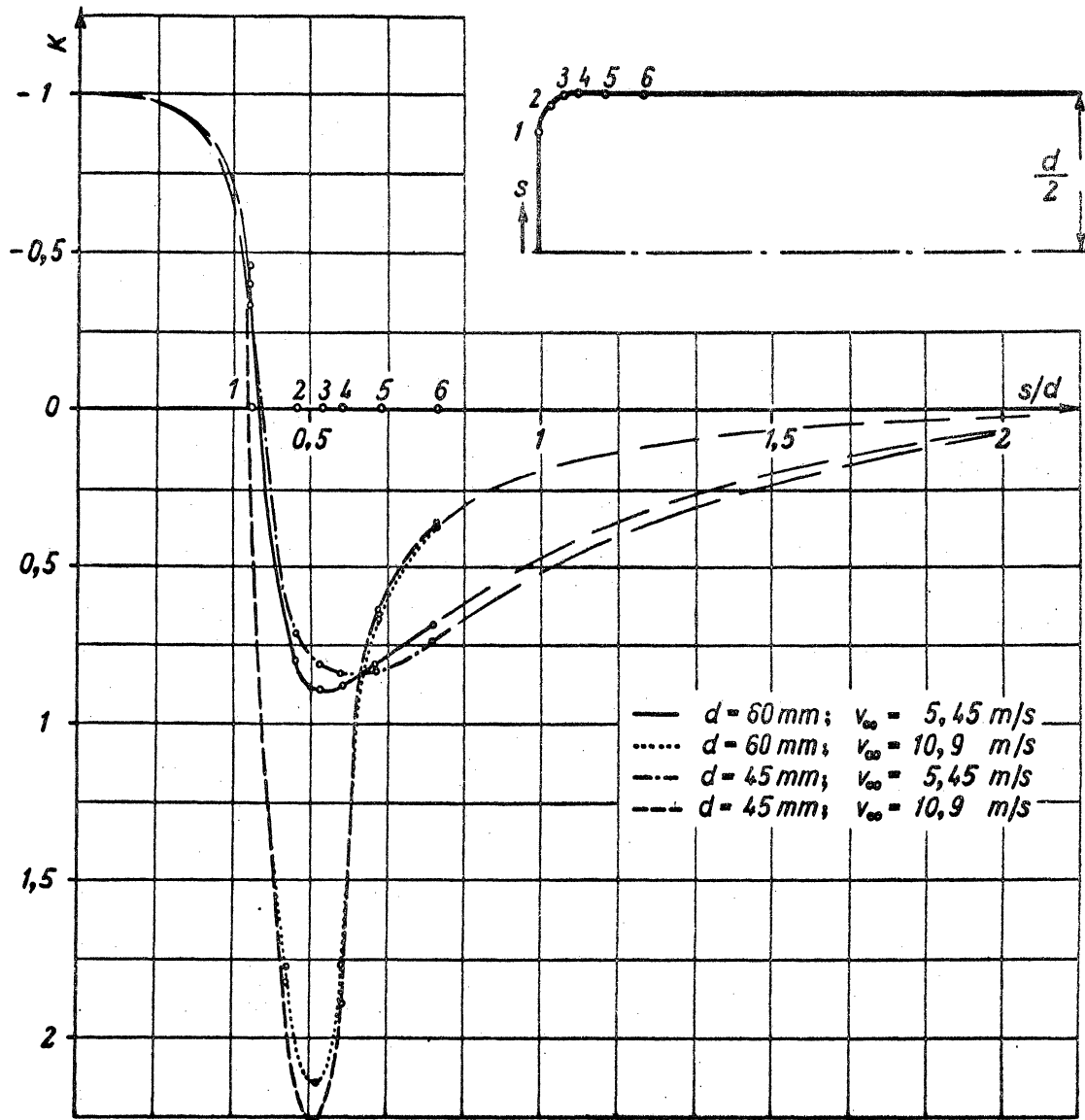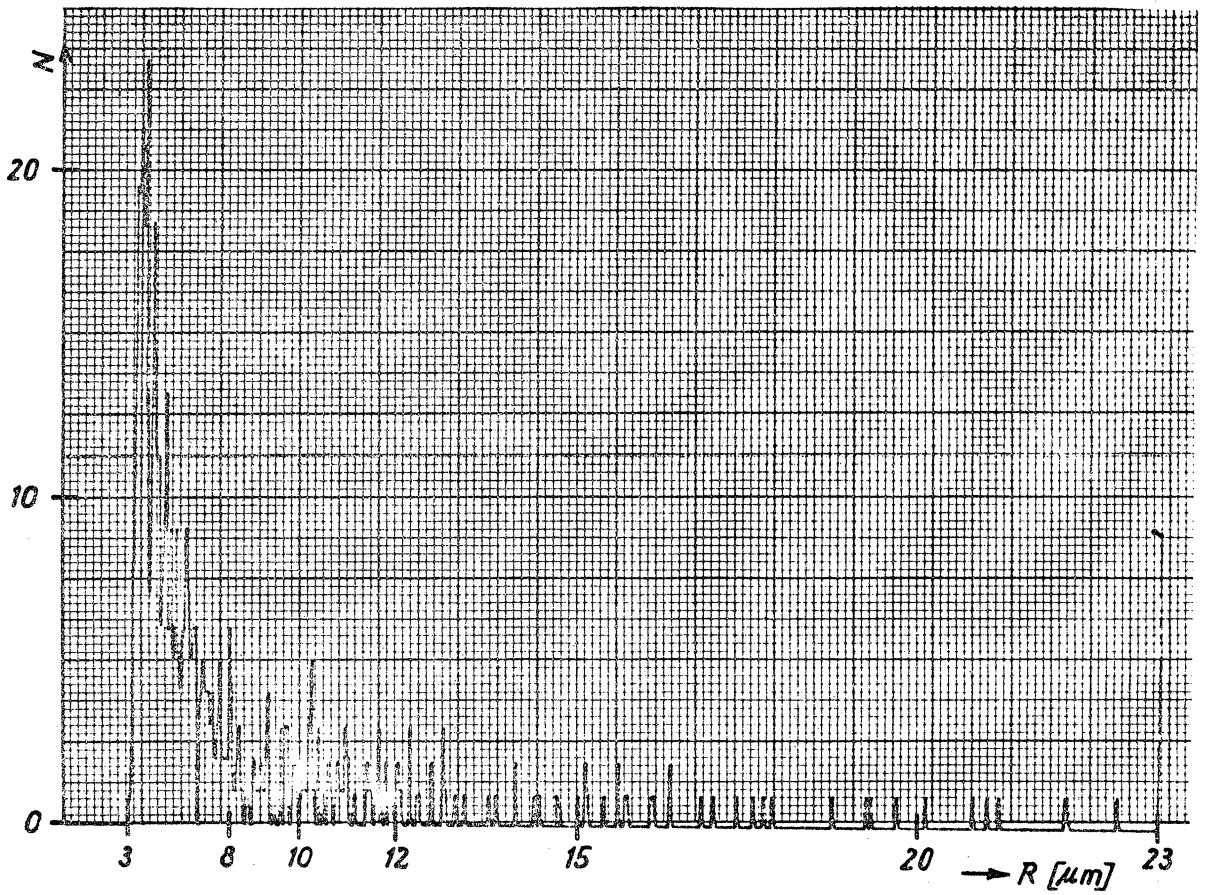Fig. 4: Dimensionless pressure distribution at the 1/2 -caliber ogive bodies
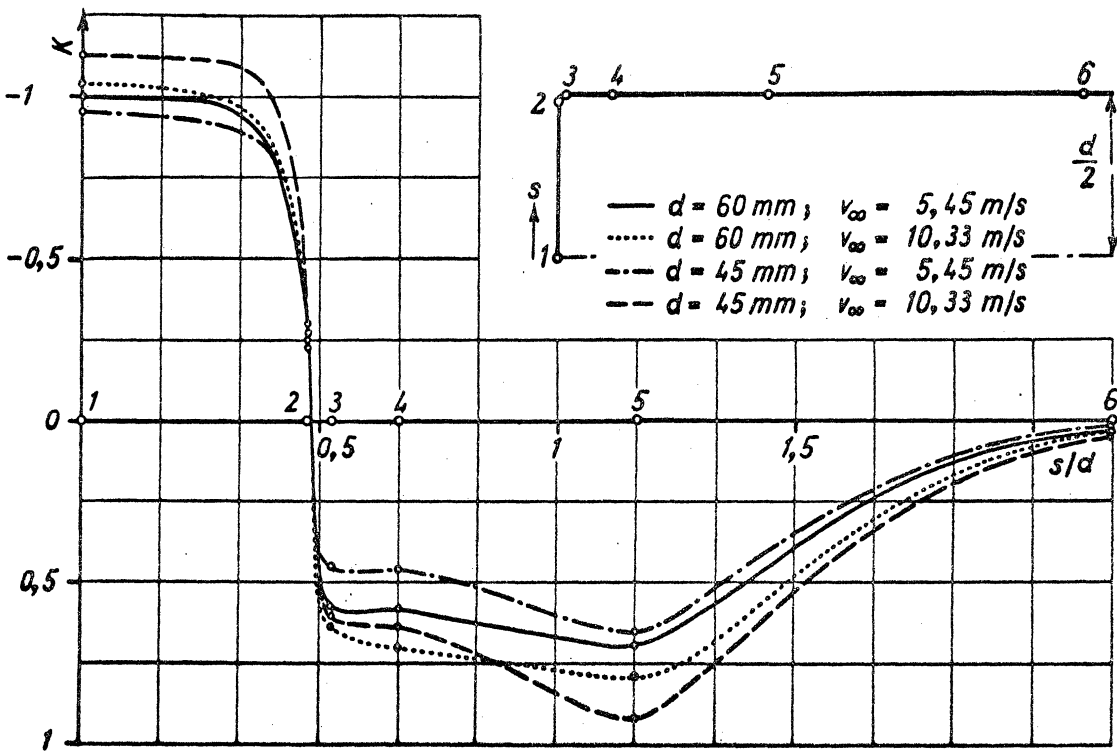
Fig. 5: Dimensionless pressure distribution at the blunt bodies
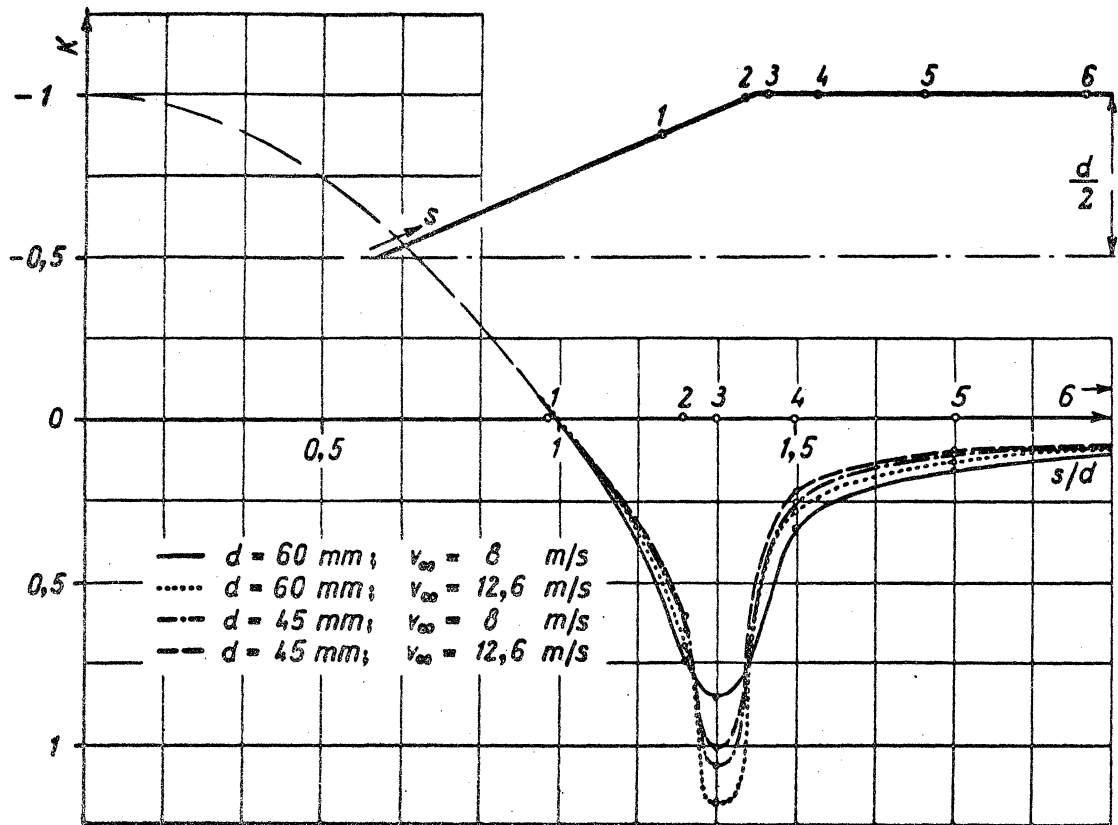
Fig. 6: Dimensionless pressure distribution at the conical bodies

Fig. 7: Dimensionless pressure distribution at the 1/8-caliber ogive bodies

Fig. 8: Nucleus size histogramm of untreatened tapwater; N_{tl}=379; N=291.5; $N_{R\ 23\ um}$ = 6.9
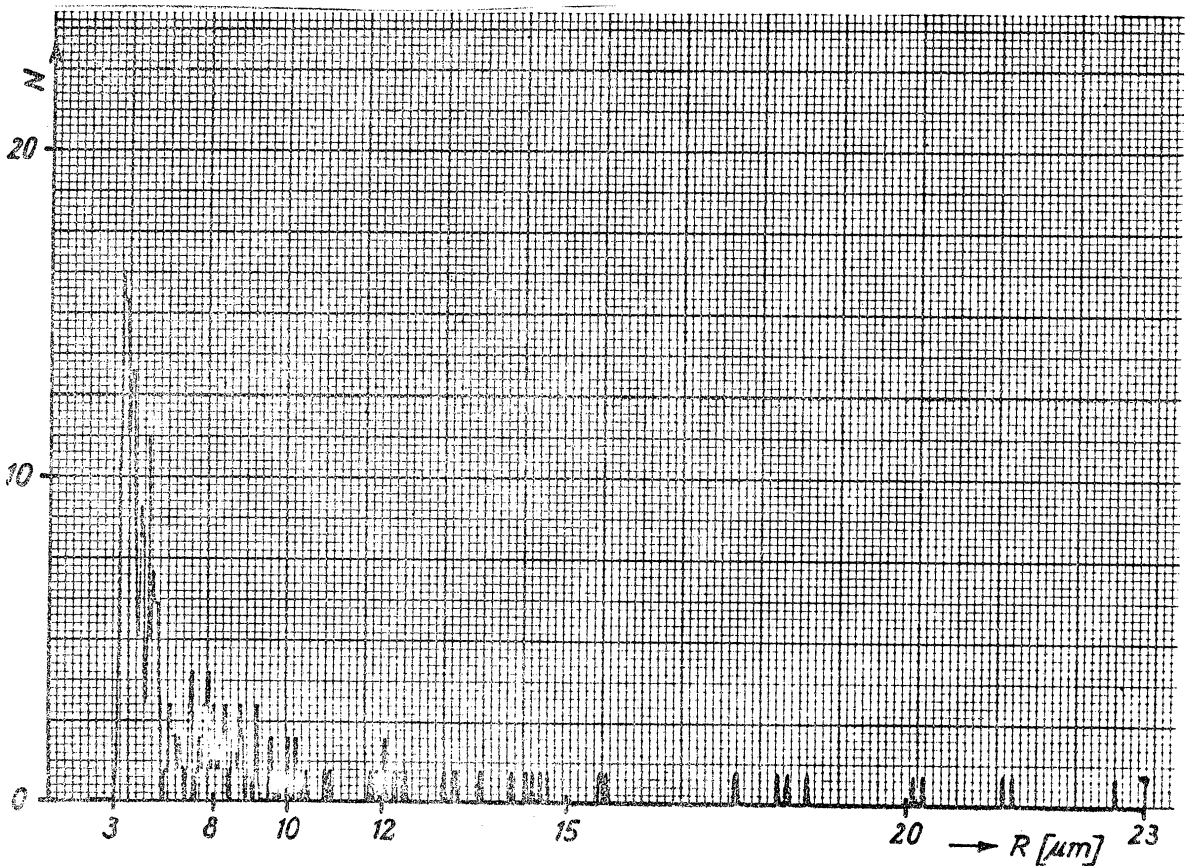
Fig. 9: Nucleus size histogram of degased tapwater (=0.35)
N_{tl}=235; N=180.8; $N_{R\ 23\ um}$=0.75
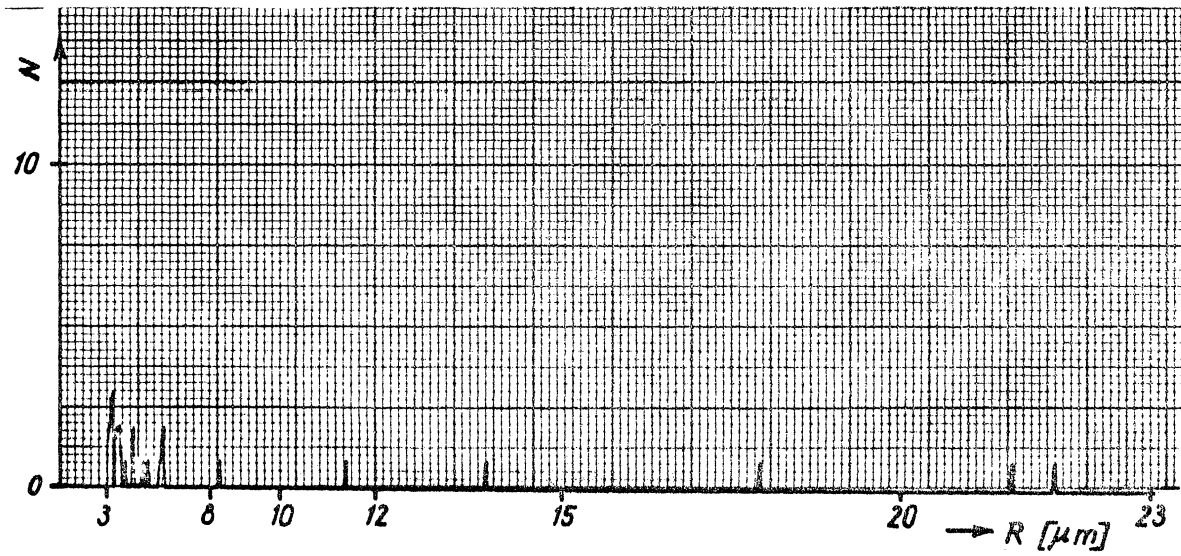
Fig. 10: Nucleus size histogram of filtered water; $N_{tl}=19$; $N=14.6$; $N_{R\ 23\ um}=0$
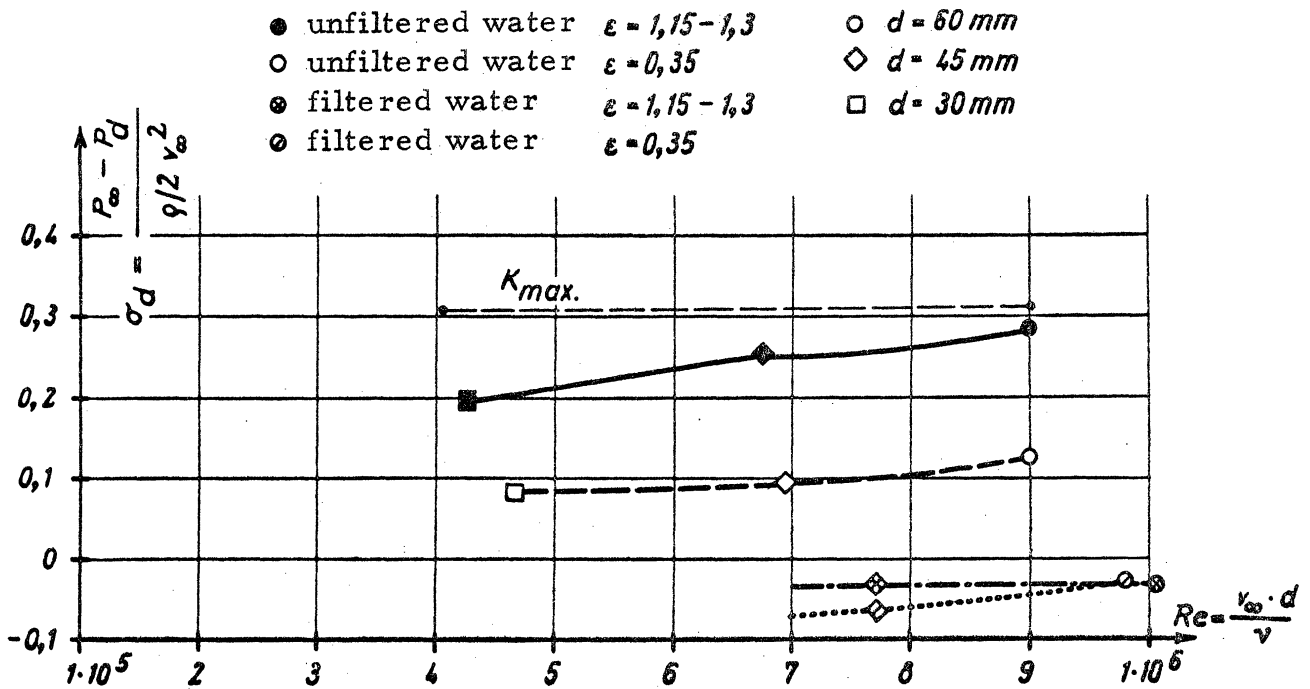
Fig. 11: Cavitation number σ_v for cavitation inception at the 2-caliber ogive shaped bodies in dependency of the Reynolds-number for diferent nucleus and gas contents. In calmed filtered water at the model body with d=30 mm no cavitation could be produced
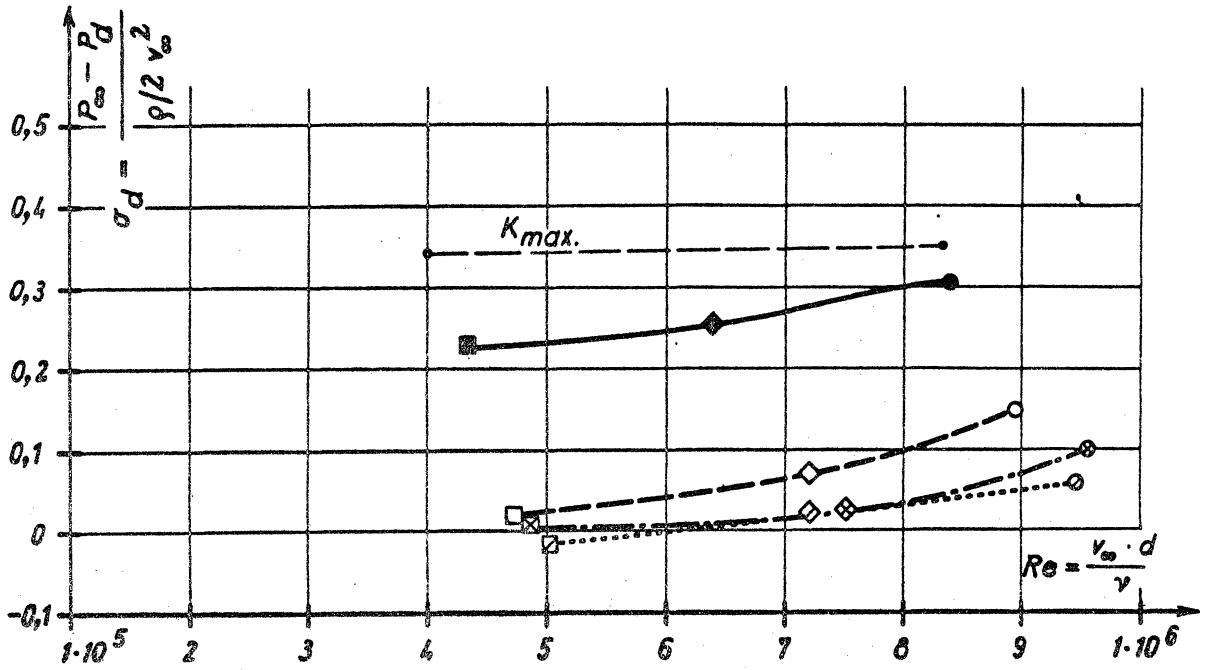
Fig. 12: Cavitation number σ_V for cavitation inception at the half body shaped bodies in dependency of the Re-number for different nucleus and gas contents
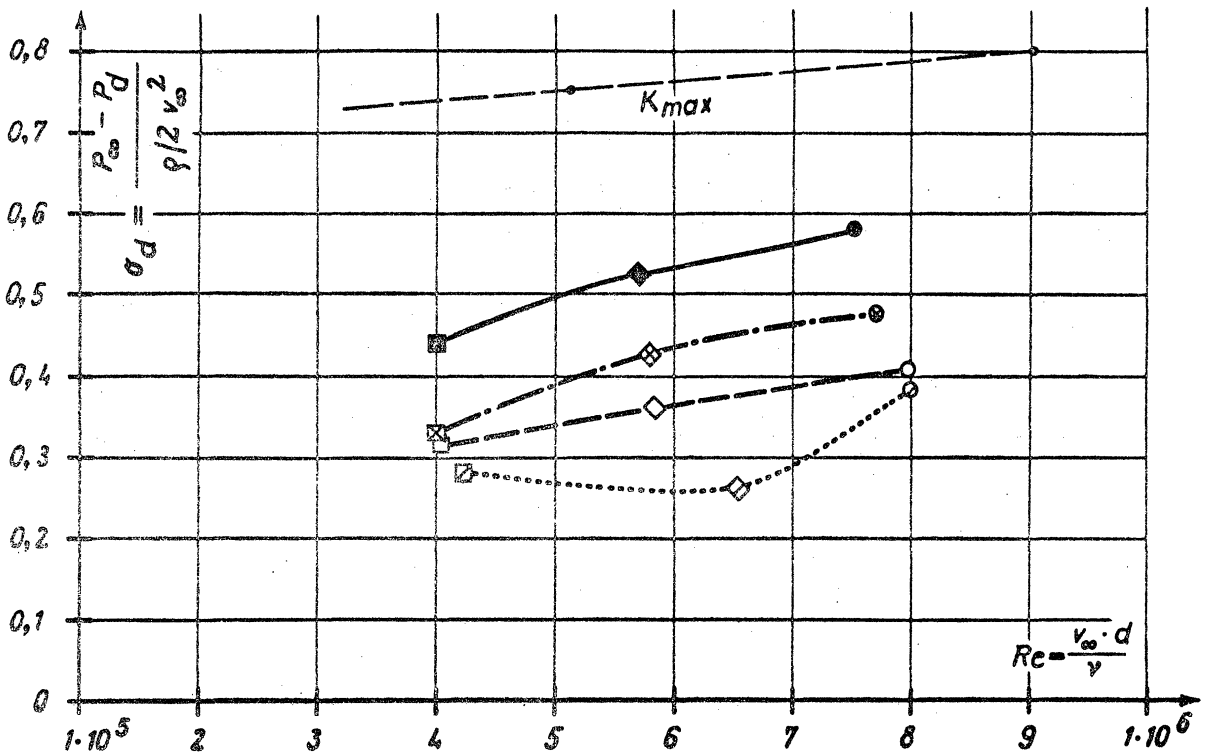
Fig. 13: Cavitation number σ_V for cavitation inception at the spherically nosed bodies in dependency of the Re-number for different nucleus and gas contents
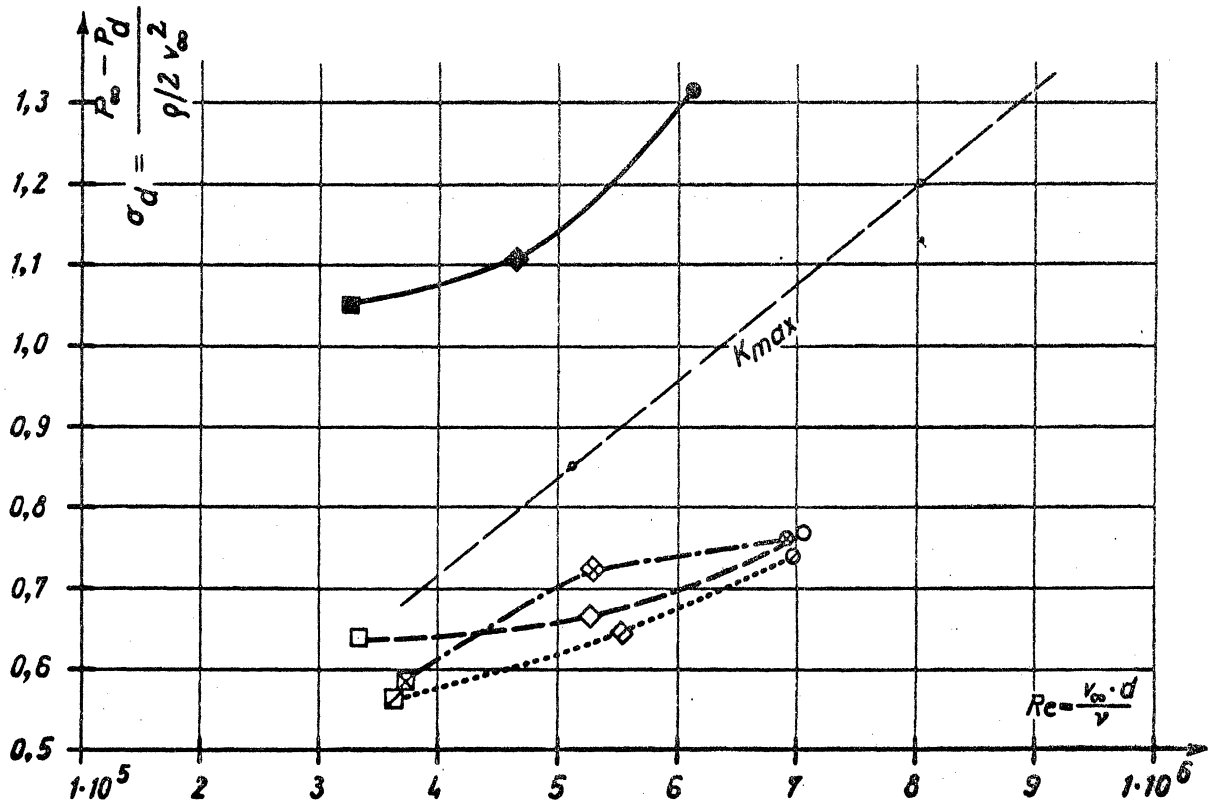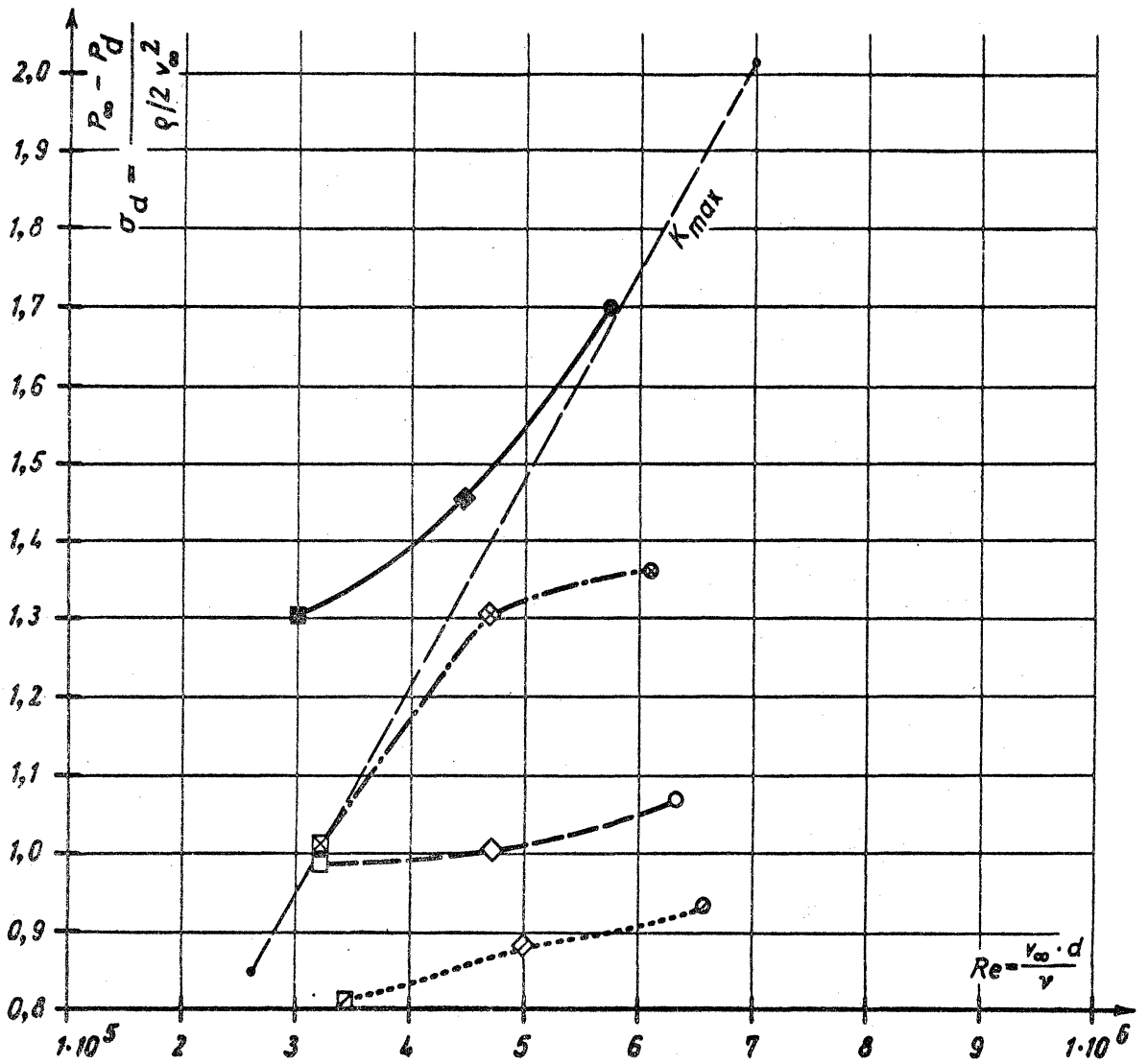
Fig. 14: Cavitation number σ_v for cavitation inception at the conically shaped bodies in dependency of the Re-number for different nucleus and gas contents

Fig. 15: Cavitation number σ_v for cavitation inception at the 1/8-caliber ogive shaped bodies in dependency of the Re-number for different nucleus and gas contents

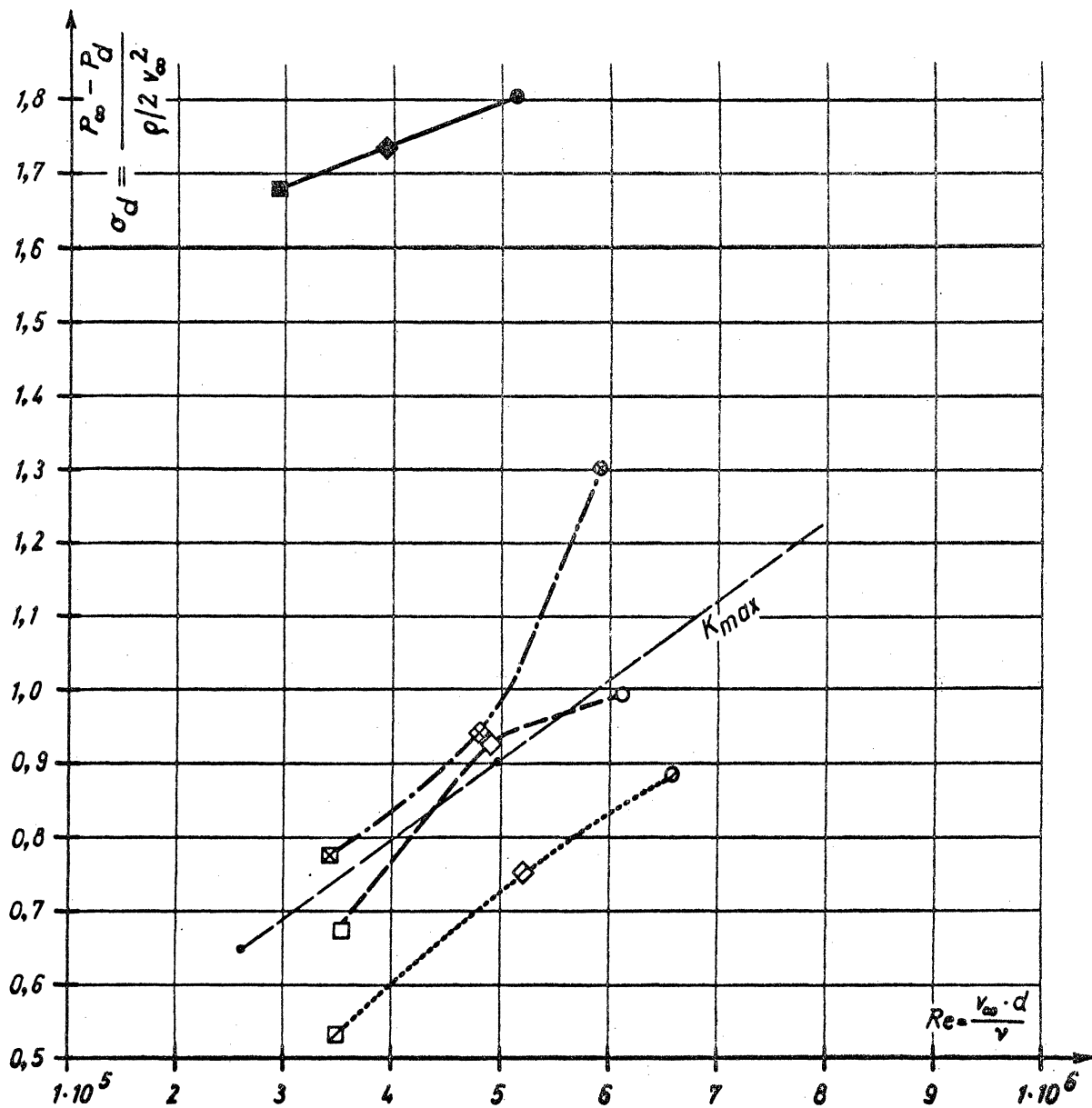Fig. 16: Cavitation number σ_v for cavitation inception at the blunt shaped bodies in dependency of the Re-number for different nucleus and gas contents
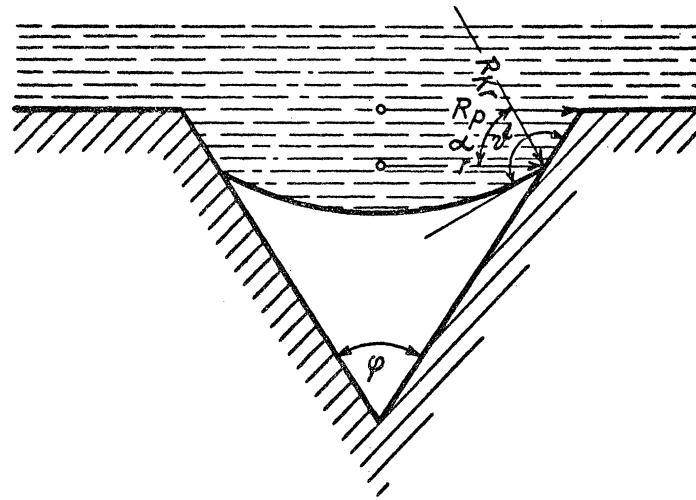
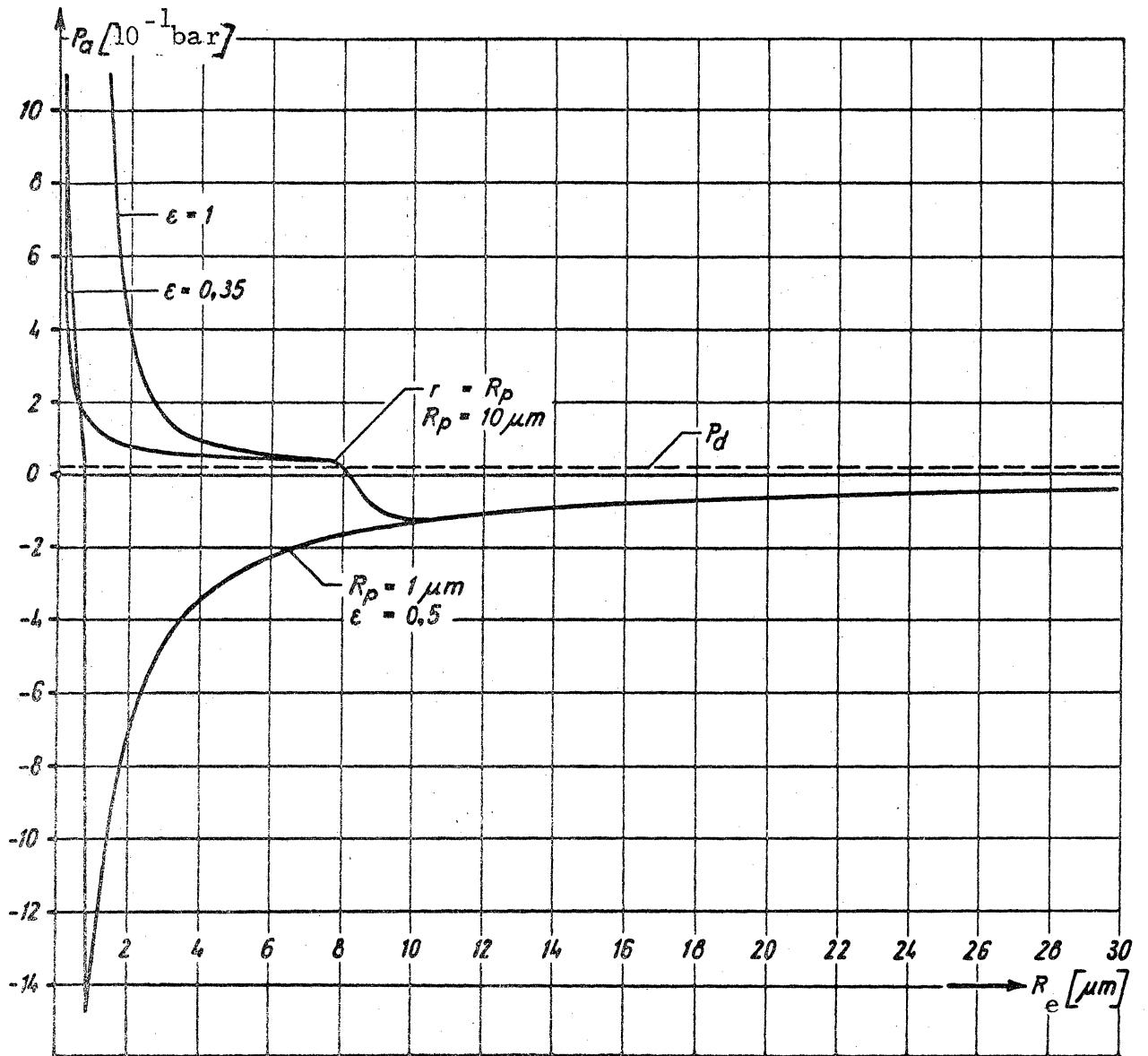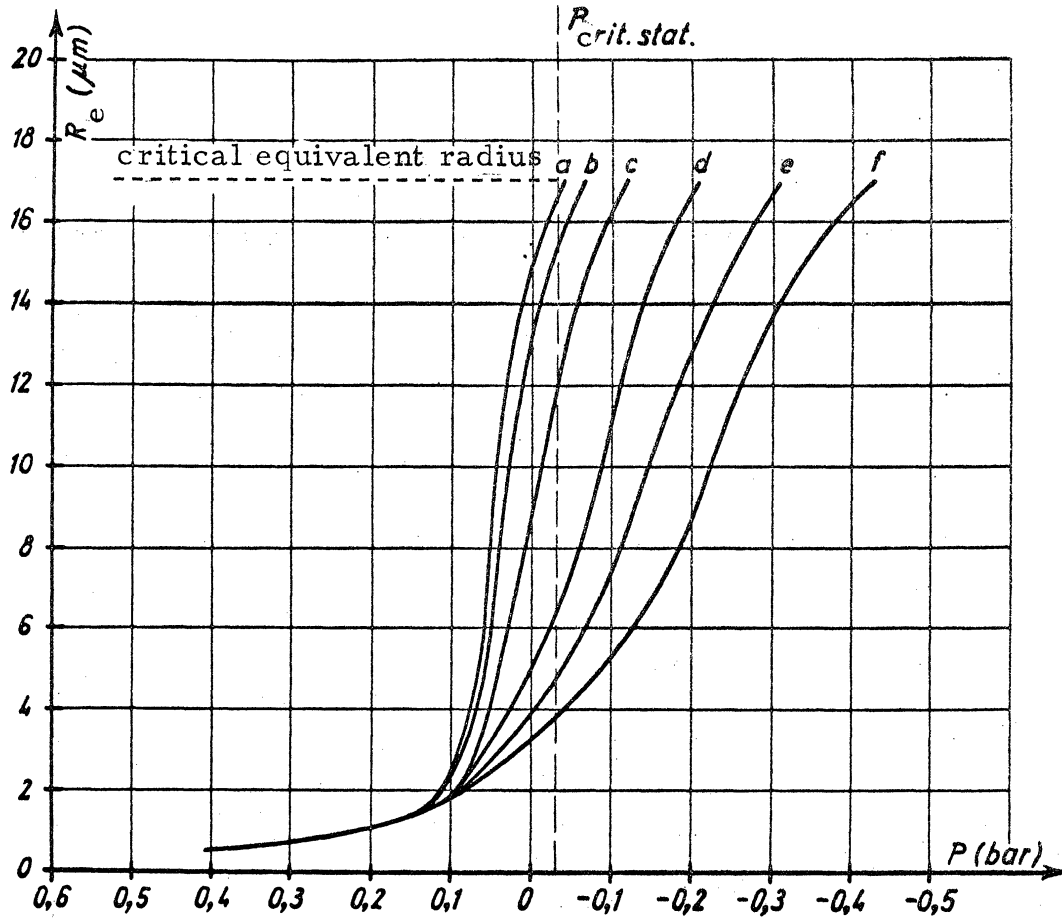Fig. 17: To the stability of conical pore nuclei

Fig. 18: Dependency of the critical pressure reduction on the pore radius R_p

curve a: half body $D = 12$ cm $R_p = 20 \mu m$; $\varepsilon = 1$; $\varphi = 100°$, $\vartheta = 150°$, $V_\infty = 14\, m/s$.
      b: " $D = 1,5$ cm   "   "   "   "   "
      c: 1/8 caliber ogive $D = 12$ cm   "   "   "   "   "
      d: " $D = 6$ cm   "   "   "   "   "
      e: " $D = 3$ cm   "   "   "   "   "
      f: " $D = 1,5$ cm   "   "   "   "   "

Fig. 19: Course of the equivalent radius of a pore with $R_p = 20 \mu m$ at different pressure gradients
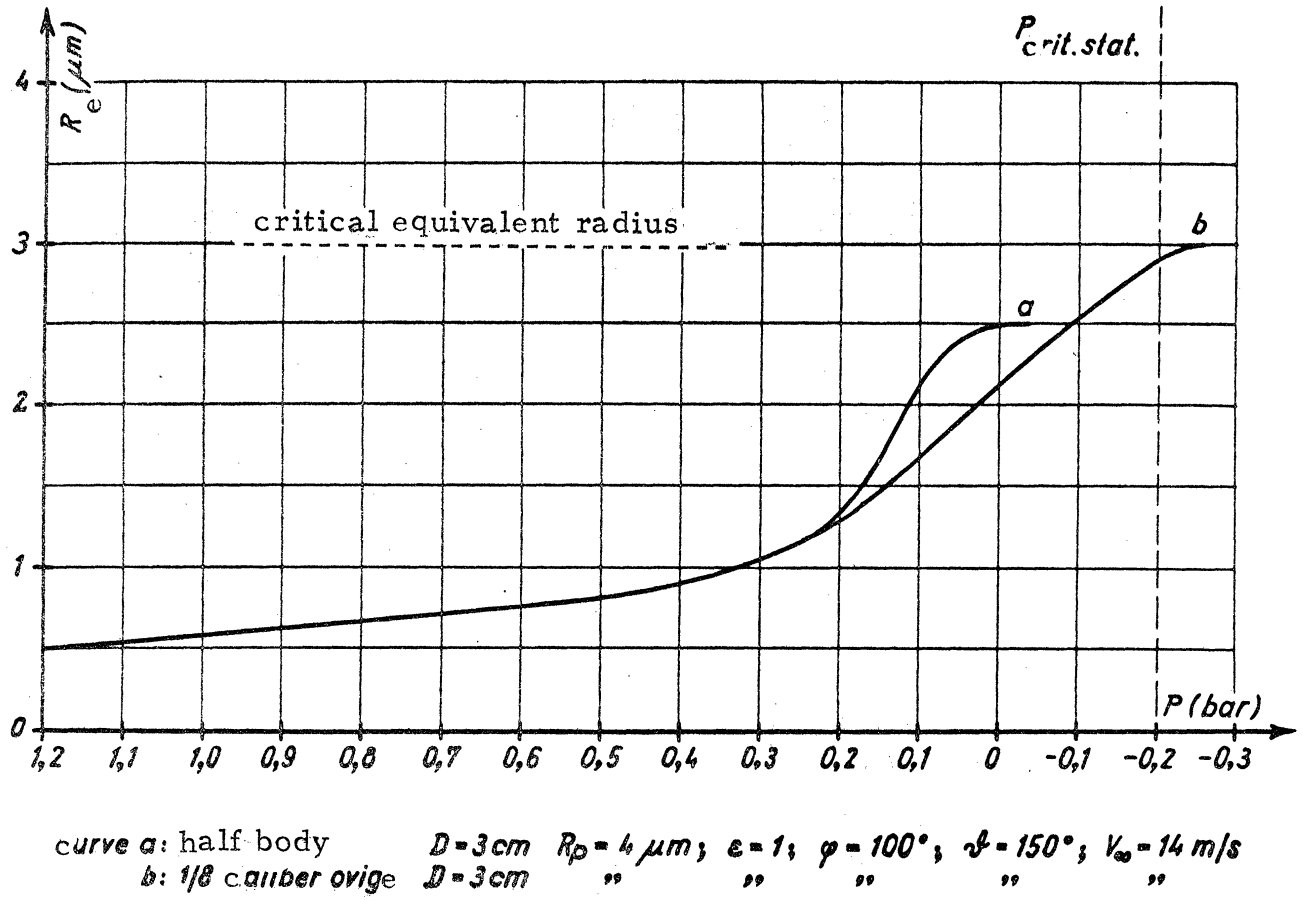
curve a: half body   D = 3 cm R_p = 4 μm ;   ε = 1 ;   φ = 100° ;   ϑ = 150° ; $V_∞$ = 14 m/s
b: 1/8 caliber ovige   D = 3 cm   „   „   „   „   „

Fig. 20: Motion of a nucleus with R_p = 4 μm at different pressure gradients